ANNUAL REVIEWS

Annual Review of Nuclear and Particle Science

The China Jinping Underground Laboratory and Its Early Science

Jian-Ping Cheng,[1] Ke-Jun Kang,[1] Jian-Min Li,[1] Jin Li,[1] Yuan-Jing Li,[1] Qian Yue,[1] Zhi Zeng,[1] Yun-Hua Chen,[2] Shi-Yong Wu,[2] Xiang-Dong Ji,[3] and Henry T. Wong[4]

[1]Key Laboratory of Particle and Radiation Imaging (Ministry of Education) and Department of Engineering Physics, Tsinghua University, Beijing 100084; email: yueq@mail.tsinghua.edu.cn, zengzhi@tsinghua.edu.cn

[2]Yalong River Hydropower Development Company, Chengdu 610051

[3]INPAC and Department of Physics and Astronomy, Shanghai Laboratory for Particle Physics and Cosmology and Shanghai Jiao Tong University, Shanghai 200240

[4]Institute of Physics, Academia Sinica, Taipei 11529; email: htwong@phys.sinica.edu.tw

Annu. Rev. Nucl. Part. Sci. 2017. 67:231–51

First published as a Review in Advance on August 7, 2017

The *Annual Review of Nuclear and Particle Science* is online at nucl.annualreviews.org

https://doi.org/10.1146/annurev-nucl-102115-044842

Keywords

underground laboratory, low-background instrumentation, dark matter searches, neutrino physics

Abstract

The China Jinping Underground Laboratory, inaugurated in 2010, is an underground research facility with the deepest rock overburden and largest space by volume in the world. The first-generation science programs include dark matter searches conducted by the CDEX and PandaX experiments. These activities are complemented by measurements of ambient radioactivity and the installation of low-background counting systems. Phase II of the facility is being constructed, and its potential research projects are being formulated. In this review, we discuss the history, key features, results, and status of this facility and its experimental programs, as well as their future evolution and plans.

Contents

1. INTRODUCTION

An established approach to the search for new physics involves experimental studies of rare-occurrence events. This typically requires low-background experiments with large target mass and elaborate shielding to suppress ambient radioactivity due to photons and neutrons. Direct and induced effects due to cosmic rays, however, cannot be shielded. Accordingly, such experiments should be performed in laboratories located underground, where a kilometer-scale rock overburden can effectively attenuate the cosmic-ray fluxes and their induced background.

Many underground facilities have been constructed around the world and house a range of diversified science programs (1). Proton decays are generic predictions of Grand Unified Theories (2, pp. 270–78) and attracted a great deal of interest in underground experiments and their techniques in the 1970s. This early phase was followed by a series of important results on neutrino oscillations and mixings (2, pp. 235–58) produced by underground experiments, which provided the first glimpse of physics beyond the Standard Model. Ongoing and future generations of long-baseline neutrino beam experiments, which also involve massive underground detectors, will advance the study of the neutrino mixing matrix. Also under way are experimental studies of neutrinoless double-β decay ($0\nu\beta\beta$) (2, pp. 698–703), which aim to demonstrate that neutrinos are Majorana particles. Beyond neutrino physics, underground laboratories are also home to an array of experiments performing direct searches for dark matter (2, pp. 353–60) in the context of weakly interacting massive particles (WIMPs, denoted by χ) and axions.

A new underground facility inaugurated in December 2010—the China Jinping Underground Laboratory (CJPL) (3, 4)—will add high-quality laboratory space to this worldwide program. In this review, we present an overview of the first-generation efforts (Phase I) at CJPL. We discuss the first science programs, particularly CDEX (China Dark Matter Experiment; 5, 6) and PandaX (Particle and Astrophysical Xenon; 7), and present their results. We then describe the associated ambient background measurements and low-counting-rate facilities at CJPL (8). We conclude with a discussion of the status and plans of Phase II (4), which is currently under construction.

2. CHINA JINPING UNDERGROUND LABORATORY: PHASE I

Since the 2000s, interest in constructing hydropower facilities in the Yalong River area of Sichuan Province, China, has intensified (9). In 2008, two 17.5-km-long traffic tunnels under Jinping

Table 1 Key features of CJPL-I and comparison with benchmark underground facilities

Facility	Location	Host structure	Access	Volume (m^3)	Rock burden/ depth (m)	Muon flux (m^{-2} day^{-1})	Start year
SNOLab (11)	Canada	Mine	Shaft	30,000	2,000	0.27	2004
Gran Sasso (10)	Italy	Traffic tunnel	Drive-in	180,000	1,400	26	1987
CJPL (3, 4)							
CJPL-I	China	Traffic tunnel	Drive-in	4,000	2,400	0.17	2010
CJPL-II	China		Drive-in	300,000	2,400		2017

Mountain were completed to facilitate the transport of construction materials. The physics community in China immediately recognized the opportunities and potential of this development. By 2009, Tsinghua University and Yalong River Hydropower Development Company had reached an agreement to jointly develop an underground laboratory facility—CJPL.

Construction of Phase I of CJPL (CJPL-I) started in December 2009 near the center of one of the Jinping traffic tunnels, where the vertical rock overburden is maximal. The inauguration of the facility took place in December 2010. **Table 1** summarizes the key features of CJPL-I and presents a comparison between this facility and the similar Gran Sasso (10) and SNOLab (11) underground facilities. **Figure 1** presents a schematic diagram of CJPL-I.

CJPL-I was built under Jinping Mountain with 2,400 m of rock overburden. It has drive-in access via a two-lane road tunnel with enough headroom for construction trucks. (The distances to the east and west ends of the tunnel entrance are 8.7 km and 8.8 km, respectively.) The main hall of CJPL-I, where the experiments were installed, has dimensions of 6.5 m (width) × 6.5 m (height) × 40 m (depth), and accordingly the floor area is 260 m^2.

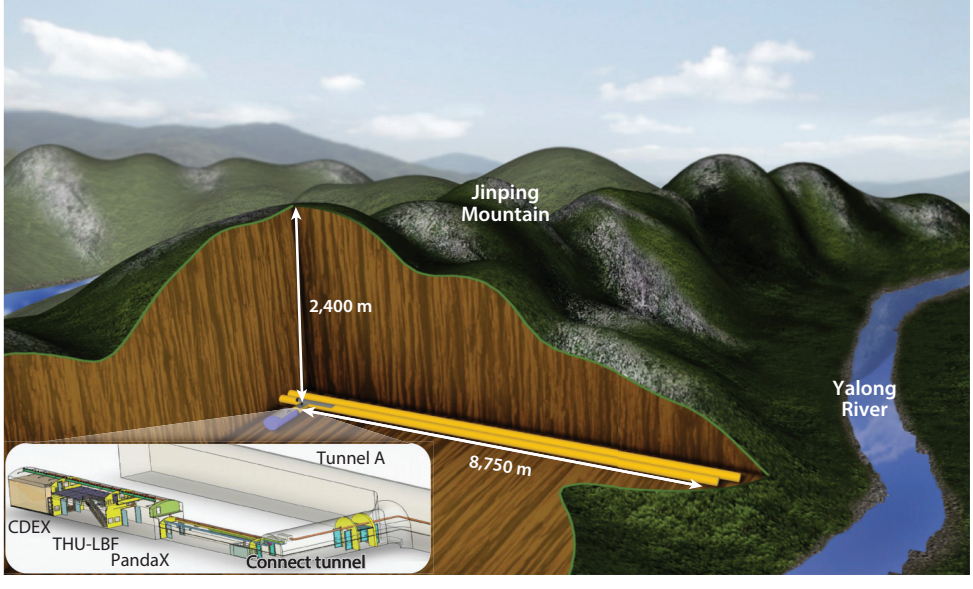

Figure 1

Schematic layout of CJPL-I, showing its geographical features and the location of the CDEX and PandaX experiments, as well as the low-background screening facilities (THU-LBF). These facilities are located in the main experiment hall, with dimensions of 6.5 m (width) × 6.5 m (height) × 40 m (length).

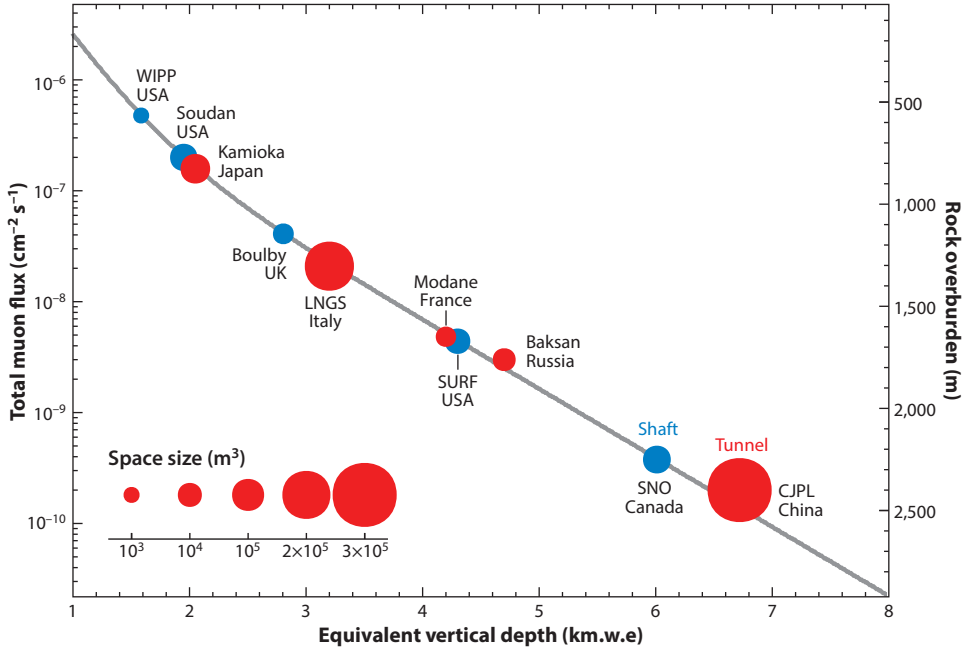

Figure 2

The measured residual muon fluxes in key underground facilities, which are consistent with predicted values (*gray line*). The sizes of the circles correspond to laboratory space by volume; red or blue denotes access by road tunnels or shafts, respectively.

The facility is the deepest operating underground laboratory in the world. The measured fluxes of residual cosmic-ray muons (12) at CJPL-I, and a comparison with various active underground laboratories, are displayed in **Figure 2**. We note for completeness that early cosmic-ray measurements were performed at the Kolar Gold Fields in India, at locations with 2,760 m of rock overburden (13).

International access to CJPL is by regular flights from various hub cities in China to Xichang Domestic Airport. The laboratory is located 90 km from the airport and is reachable by both highways and paved two-lane private roads shared with Yalong River Hydropower Development Company; the driving time is approximately 2 hours. A guest house, dormitory accommodation, canteens, and office space are available near the west entrance of the tunnel.

The bedrock surrounding CJPL is made of marble, with relatively low radioactivity from the contamination of ^{232}Th and ^{238}U isotopes (measurements of these isotopes and other background characterizations are discussed in Section 5). The laboratory space is shielded from the bare rock by a 0.5-m-thick layer of concrete. Ventilation is provided by a 10-km-long, 55-cm-diameter pipeline that brings in fresh air from the west entrance of the tunnel at an air-exchange rate of 4,500 $m^3\ h^{-1}$, allowing the radon level to be kept below 20 Bq m^{-3}.

The laboratory is connected by internet cables at a bandwidth of 10 GHz. The storage capacity of the computer servers, located in an exterior office, is up to 300 TB, with a transfer capacity of 10 GHz from the experiments. The laboratory is equipped with surveillance CCD cameras and audiovisual alarm systems, and ambient conditions including temperature, pressure, humidity, and air composition are continually recorded. All recording devices are accessible from and can be monitored at remote sites.

The CJPL-I laboratory space is shared among three scientific programs: the CDEX (5) and PandaX (7) dark matter experiments and the Tsinghua University low-background facilities (THU-LBF) for low-radiopurity measurements (8). The status and early results of these programs are discussed in the following sections.

3. CDEX

Approximately one-quarter of the energy density of the Universe can be attributed to cold dark matter (2, p. 353), whose nature and properties are unknown. WIMPs are leading candidates. They interact with matter predominantly via elastic scattering with nuclei: $\chi + N \rightarrow \chi + N$. The unique merits of CJPL make it an ideal location in which to perform low-background experiments on dark matter searches.

Germanium detectors sensitive to sub-keV recoil energy are a possible means of probing so-called light WIMPs with mass 1 GeV $< m_\chi <$ 10 GeV (14, 15). This observation inspired detailed studies of *p*-type point-contact germanium (pPCGe) detectors with modular mass on the kilogram scale (16–18), which were followed by various experimental efforts (19–23). The scientific goal of CDEX (5), one of the two founding experimental programs at CJPL, is to pursue studies of light WIMPs with pPCGe.

3.1. First-Generation CDEX Experiments

The first-generation CDEX experiments adopted a baseline design (21, 22) of single-element 1-kg mass scale pPCGe detectors enclosed in NaI(Tl) crystal scintillator as anti-Compton (AC) detectors (**Figure 3**). These active detectors are surrounded by passive shielding made of

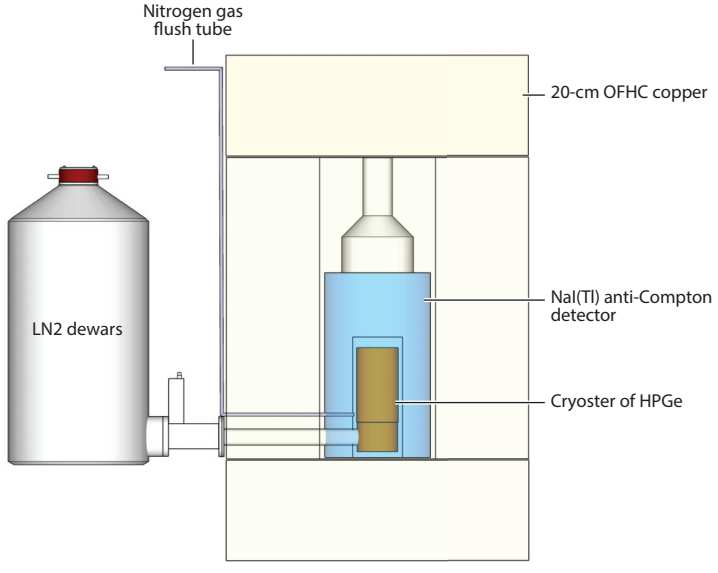

Figure 3

Schematic diagram of the baseline design of the CDEX-0 and CDEX-1 experiments, which use a *p*-type point-contact germanium detector enclosed by anti-Compton NaI(Tl) crystal scintillator and passive shielding. This setup is further shielded by an external structure (not shown) made of lead and copper layers. The entire shielding and detector system is installed inside a room with 1-m-thick polyethylene walls. Abbreviations: HPGe, high-purity germanium detector; OFHC, oxygen-free high-conductivity.

oxygen-free high-conductivity (OFHC) copper, boron-loaded polyethylene, and lead. The setup is further shielded by additional OFHC copper and lead layers. The entire shielding and detector system is installed inside a room with interior dimensions of 4 m × 8 m × 4 m (height) and walls constructed with 1-m-thick polyethylene.

The pilot CDEX-0 measurement was based on a 20-g prototype germanium detector at a 177-eV_{ee} threshold with an exposure of 0.784 kg·day (25). The CDEX-1 experiment adopted a pPCGe detector with a mass of 1 kg. The first results [without the NaI(Tl) AC detector] were based on an analysis threshold of 400 eV_{ee} with an exposure of 14.6 kg·day (26, 27). Subsequent data taking incorporated the AC detector. After suppression of the anomalous surface background events and measurement of their signal efficiencies and background leakage factors with calibration data (28, 29), all residual events were accounted for by known background models. The sensitivities were further improved with a longer exposure of 335.6 kg·day, and new constraints on spin-independent and spin-dependent WIMP–nucleon (χN) couplings were derived (24). The results (**Figure 4**) represent the most sensitive measurements made with the point-contact high-purity germanium (HPGe) detector.

Figure 5*a* shows the dark matter constraints on χN spin-independent cross sections, along with other selected benchmark results (20, 30–36). In particular, the allowed region from the CoGeNT experiment (20) was probed and excluded by the CDEX-1 results. The anomalous excess originated from the leakage of surface events into the bulk signal samples (28). **Figure 5*b*** shows the constraints on WIMP–neutron (χn) spin-dependent cross sections, which also represent an improvement over published results in the light-WIMP region (30, 37, 38).

The superb energy resolution of germanium detectors allows spectral structures to be resolved even at low energies, where atomic-physics effects can be important. This benefits studies of axion-like particles (39) because these particles' experimental signatures are usually manifested as peaks or steps in their energy depositions at the target. An analysis was performed with the CDEX-1 data, and constraints on axion–electron couplings (g_{Ae}) for solar (**Figure 5*c***) and dark matter axions (**Figure 5*d***) were derived (40). In particular, the data represent an improvement over earlier results (41, 42) for dark matter axions with mass below 1 keV.

The CDEX-1 data set is currently being analyzed with a yearlong exposure. Studies of annual modulation effects, as well as other physics channels, are under way. New data are being taken with an upgraded pPCGe detector with a lower threshold.

3.2. Current Efforts and Future Goals

The long-term goal of the CDEX program is a ton-scale germanium experiment (CDEX-1T) searching for dark matter and $0\nu\beta\beta$ (2, pp. 698–703). A pit with a diameter of 18 m and a height of 18 m has been built in Hall C of CJPL Phase II (CJPL-II) to house such an experiment (**Figure 6*a***).

Toward this end, the so-called CDEX-10 prototype has been constructed with detectors in an array structure with a target mass in the 10-kg range. CDEX-10 will provide a platform to study the many issues involving scaling up in detector mass and in improvement of background and threshold. The detector array is shielded and cooled by liquid nitrogen (liquid argon may be investigated in the future, as it may offer an additional benefit of active shielding for AC detectors).

Researchers are also pursuing other crucial technology acquisition projects that would make a ton-scale germanium experiment realistic and feasible. These include (*a*) detector-grade germanium crystal growth; (*b*) germanium detector fabrication; (*c*) development of an ultralow-background, low-temperature, low-noise preamplifier; and (*d*) production of electroformed copper, expected to be eventually performed underground at CJPL.

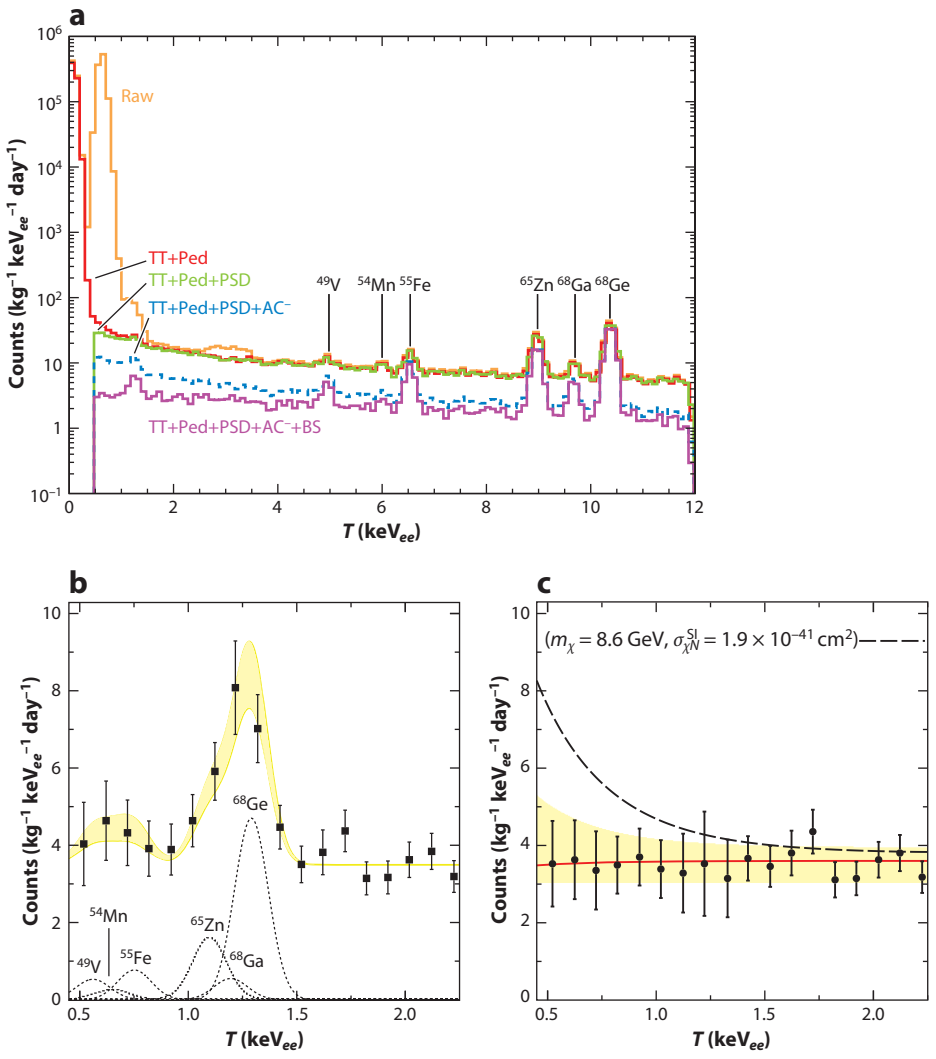

Figure 4

Background spectra of the CDEX-1 experiment with 335.6 kg·day of exposure (24). (*a*) Spectra at various stages of candidate event selection: basic cuts (TT+Ped+PSD), anti-Compton (AC), and bulk (BS) events. The peaks correspond to internal X-ray emission from cosmogenically activated long-lived isotopes. (*b*) Low-energy candidate events can be accounted for with known background channels: L-shell X-rays from internal cosmogenic radioactivity and a flat background due to ambient high-energy γ-rays. (*c*) The residual spectrum superimposed with a hypothetical weakly interactive massive particle (WIMP)–nucleon (χN) recoil spectrum in an excluded parameter space.

The first detector fabricated from commercial crystal that matches expected performance will be installed at CJPL in 2017. This detector enables control of assembly materials placed in its vicinity that are known to be the dominant source of radioactive background, as well as efficient testing of novel electronics and readout schemes. The benchmark would be the ability to perform light-WIMP searches with germanium detectors having $0\nu\beta\beta$-grade background control. This configuration would enable detailed studies of potential cosmogenic tritium contamination in

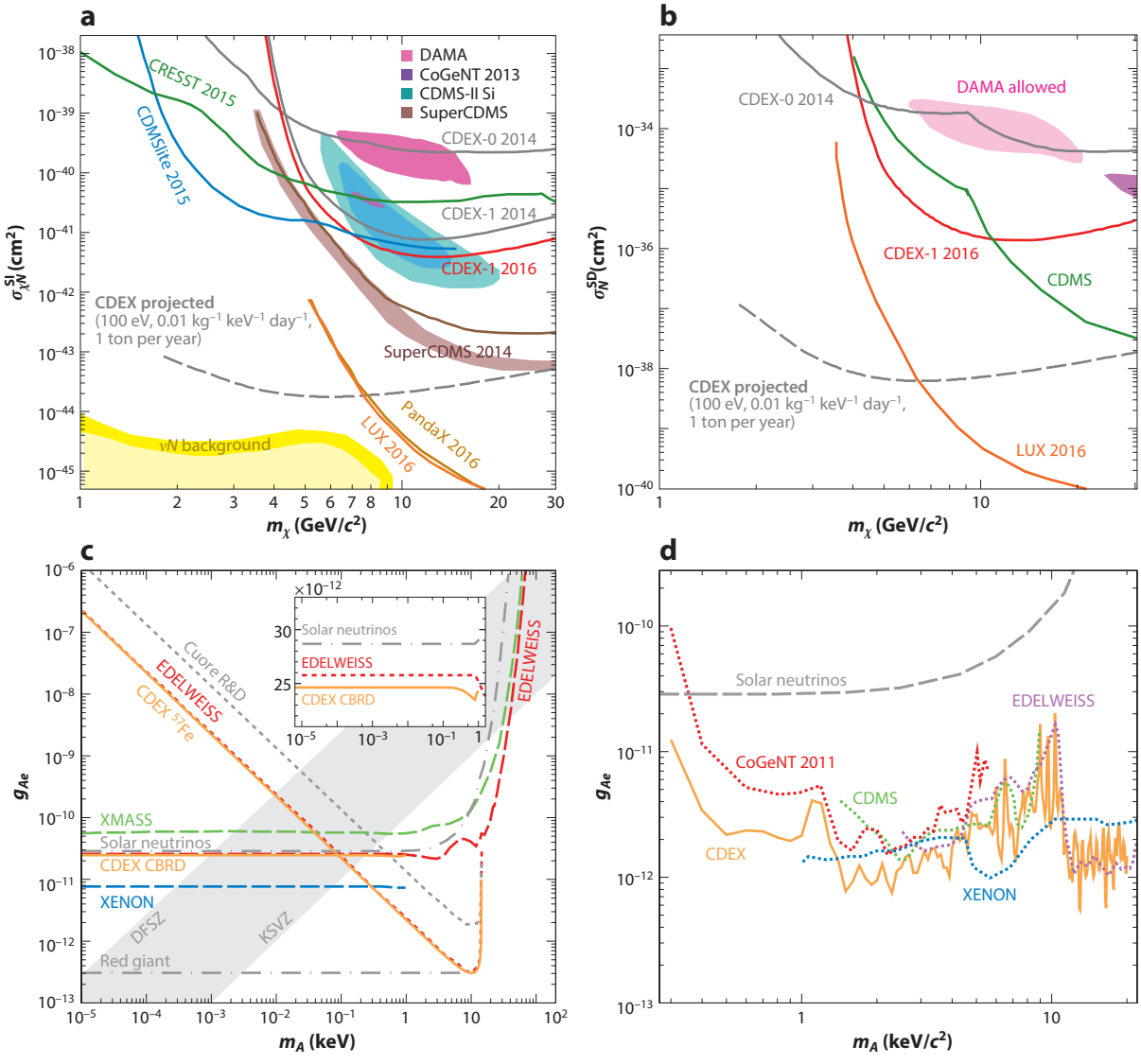

Figure 5

Regions in couplings versus the weakly interacting massive particle (WIMP) mass parameter space probed and excluded by the CDEX-1 experiment with 335.6 kg·day of exposure, along with comparisons with other benchmark results. (*a*) Spin-independent WIMP–nucleon (χN) couplings (24). (*b*) Spin-dependent WIMP–neutron (χn) couplings (24). (*c*) Axion–electron (*Ae*) couplings with solar axions (40). (*d*) *Ae* couplings with dark matter axions (40).

germanium detectors, which in turn would allow the exploration of strategies to suppress such background.

The projected sensitivities to χN spin-independent (**Figure 5*a***) and spin-dependent cross sections (**Figure 5*b***) for CDEX-1T at targeted specifications in the detector threshold, background levels, and data size. The goal of the $0\nu\beta\beta$ program will be to achieve sufficient sensitivities to completely cover the inverted neutrino mass hierarchy. The first $0\nu\beta\beta$ analysis of the CDEX-1

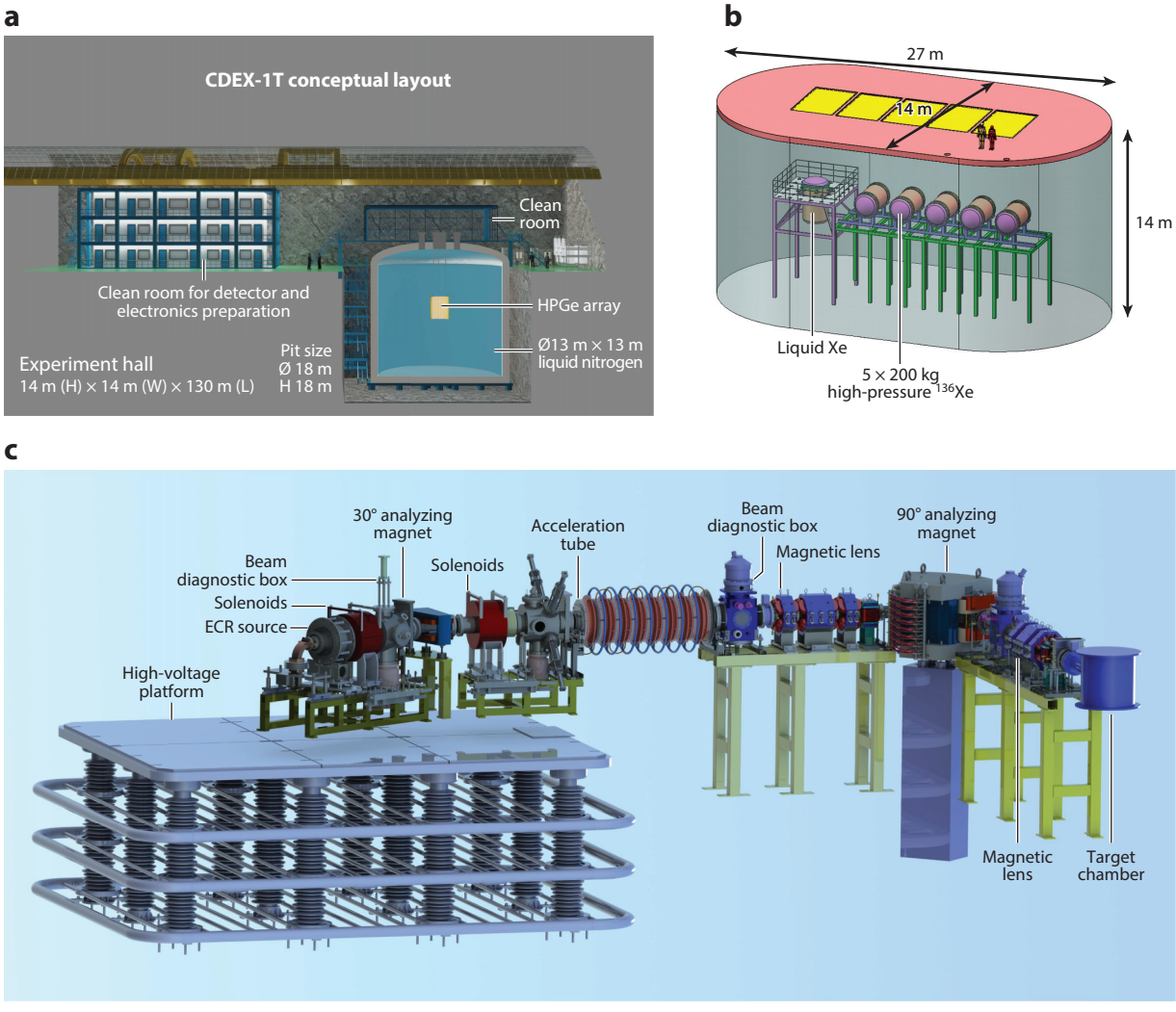

Figure 6

Schematic and conceptual layout of the three ongoing research programs expected to be installed at CJPL-II: (*a*) CDEX, (*b*) PandaX, and (*c*) JUNA. (*a*) CDEX and (*b*) PandaX conduct searches for dark matter and neutrinoless double-β decay in Hall C and Hall B, respectively. (*c*) JUNA focuses on low-counting accelerator-based nuclear physics and astrophysics measurements in Hall A. Abbreviations: ECR, electron cyclotron resonance; HPGe, high-purity germanium detector.

data has been performed, and an upper limit of $\tau_{1/2} > 6.4 \times 10^{22}$ year at the 90% confidence level was derived (43).

4. PandaX

The PandaX program (3, 4) uses xenon as the target and detector medium in searches for WIMP dark matter, as well as for $0\nu\beta\beta$ in ^{136}Xe isotopes. The program follows a staged plan. The first and second stages (PandaX-I and -II) focus on WIMP detection at CJPL-I (3, 4), whereas the

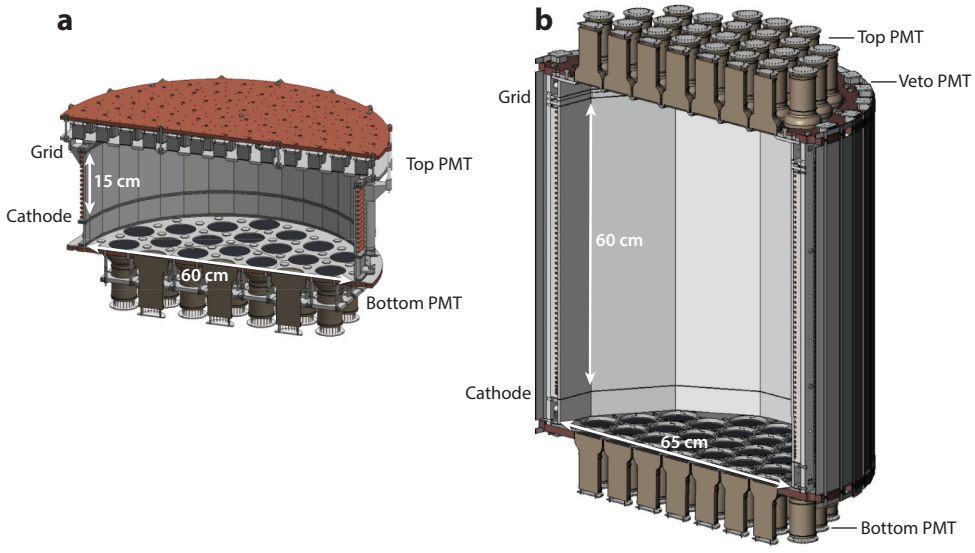

Figure 7

The basic features of the PandaX-I and PandaX-II experiments. (*a*) The time-projection chamber (TPC) for PandaX-I, with a small drift length of 15 cm between the cathode and anode grid. (*b*) The TPC for PandaX-II, with a significantly greater drift length of 60 cm. Abbreviation: PMT, photomultiplier tube.

future PandaX-III (a $0\nu\beta\beta$ experiment) and -IV (a multiton xenon dark matter experiment) will be installed at CJPL-II (4).

4.1. Dark Matter Searches with PandaX-I and PandaX-II

Both PandaX-I and -II utilize a so-called dual-phase xenon time-projection chamber (TPC) to study recoil signals from xenon nuclei upon interaction with WIMPs. Two types of signals, S1 and S2, are recorded for every event. They are produced by scintillation photons and ionization electrons, respectively. The XENON (44, 45), ZEPLIN (46), and LUX (36) experiments have demonstrated that the liquid xenon detector techniques offer exceptional potential for background suppression and discrimination, as well as scalability to high target mass, leading to WIMP detection sensitivity in a wide mass range.

PandaX-I and -II share a common infrastructure (**Figure 7**), described in detail in Reference 7. Passive shielding consisting of polyethylene, lead, and copper was constructed to suppress ambient neutrons and γ-rays. The innermost shield is a vacuum copper vessel that is also a vacuum jacket for the cryostat, as well as a radon barrier. The cryogenic and gas handling systems (47) store, circulate, and cool the xenon, and have enough capacity for a ton-scale experiment.

PandaX-I (**Figure 7*a***) (7, 48) was a 120-kg liquid xenon TPC with polytetrafluoroethylene (PTFE) reflective walls to enhance light collection. Its top and bottom photomultiplier tube (PMT) arrays consisted of, respectively, 143 and 37 PMTs with diameters of 1 and 3 inches that collected the S1 and S2 photons from events originating in the active volume. The upgrade to PandaX-II (**Figure 7*b***) includes a new low-background steel inner vessel, an increased liquid xenon target mass of 580 kg, and a total of 110 3-inch-diameter PMTs. An additional 48 1-inch-diameter PMTs serve as an active veto in the optically isolated 4-cm liquid xenon region surrounding the outer circumference of the TPC, providing extra power for background rejection (49).

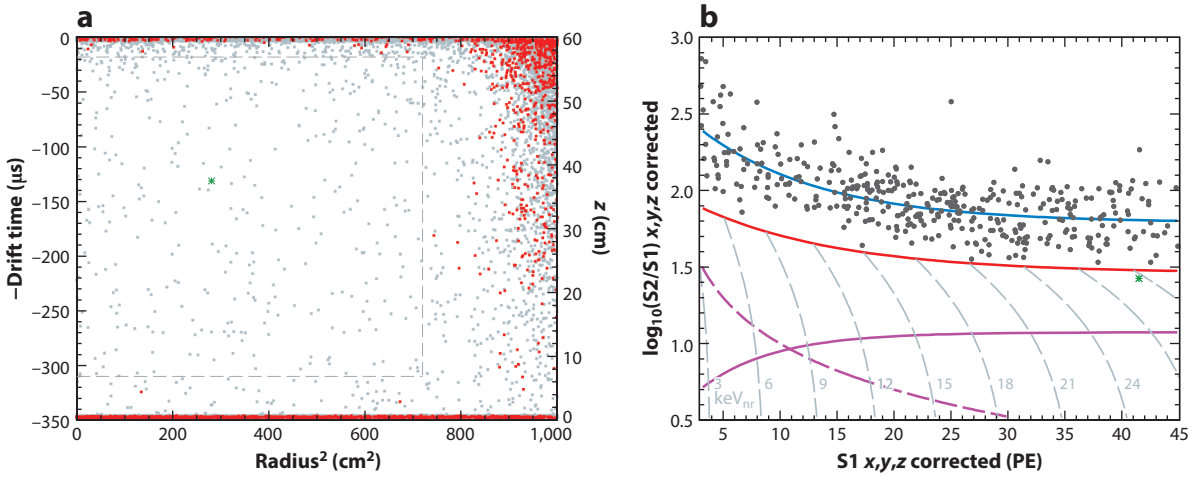

Figure 8

Event distributions from the PandaX-II data. (*a*) Spatial distribution of the events and the defined fiducial volume to select candidate events. (*b*) The band of $\log_{10}$(S2/S1) versus S1 from PandaX-II events within the fiducial volume. The red solid line represents the fitted median derived from nuclear recoil calibration data. Weakly interacting massive particle candidate signals are those below the median line; no such events were observed.

Candidate events from χN elastic scattering are selected according to their locations in the central fiducial volume (**Figure 8*a***). In addition, correlations of the S1 and S2 signatures allow differentiation of nuclear recoil events versus electron recoil background. **Figure 8*b*** shows the $\log_{10}$(S2/S1) band of potential signal events, along with calibration data with a neutron source.

The PandaX-I experiment collected data for dark matter searches between May and October 2014. The final results from PandaX-I,with a total exposure of 54 × 80.1 kg·day, are presented in Reference 50. The data distribution is consistent with the background-only hypothesis. A profile likelihood analysis was performed with all candidate events and the expected WIMP and background distributions, leading to the exclusion limit of the χN spin-independent elastic scattering cross section shown in **Figure 9*a***. At the 90% confidence level, the results are incompatible with the spin-independent isoscalar WIMP interpretation of all previously reported positive signals from the DAMA/LIBRA (30, 51, 52), CoGeNT (19, 20), CRESST-II (53), and CDMS-II-Si (32) experiments. The bounds on the χN cross section are more stringent than those from SuperCDMS (33) above a WIMP mass of 7 GeV/c^2. Below a mass of 5.5 GeV/c^2, the results were the tightest reported constraints among all xenon-based experiments.

The upgrade from PandaX-I to PandaX-II was completed in 2015. The physics commissioning run performed from November to December 2015 obtained a dark matter exposure of 306 × 19.1 kg·day. The data taking concluded with the identification of a strong ^{85}Kr background. The analysis of this data set has been published (49). No WIMP candidates were identified, and a 90% upper limit comparable to the 225-day limit from XENON100 (45) was set. PandaX-II resumed physics data taking in March 2016 after a krypton distillation campaign that reduced the krypton level by a factor of 10, leading to an average electron-recoil background of 2×10^{-3} events (kg·day)$^{-1}$—the world's lowest reported level. The combined data from the commissioning run and an additional data-taking period from March to June 2016 provide a total exposure of 3.3×10^4 kg·day (54) and represent the largest WIMP search data set to date.

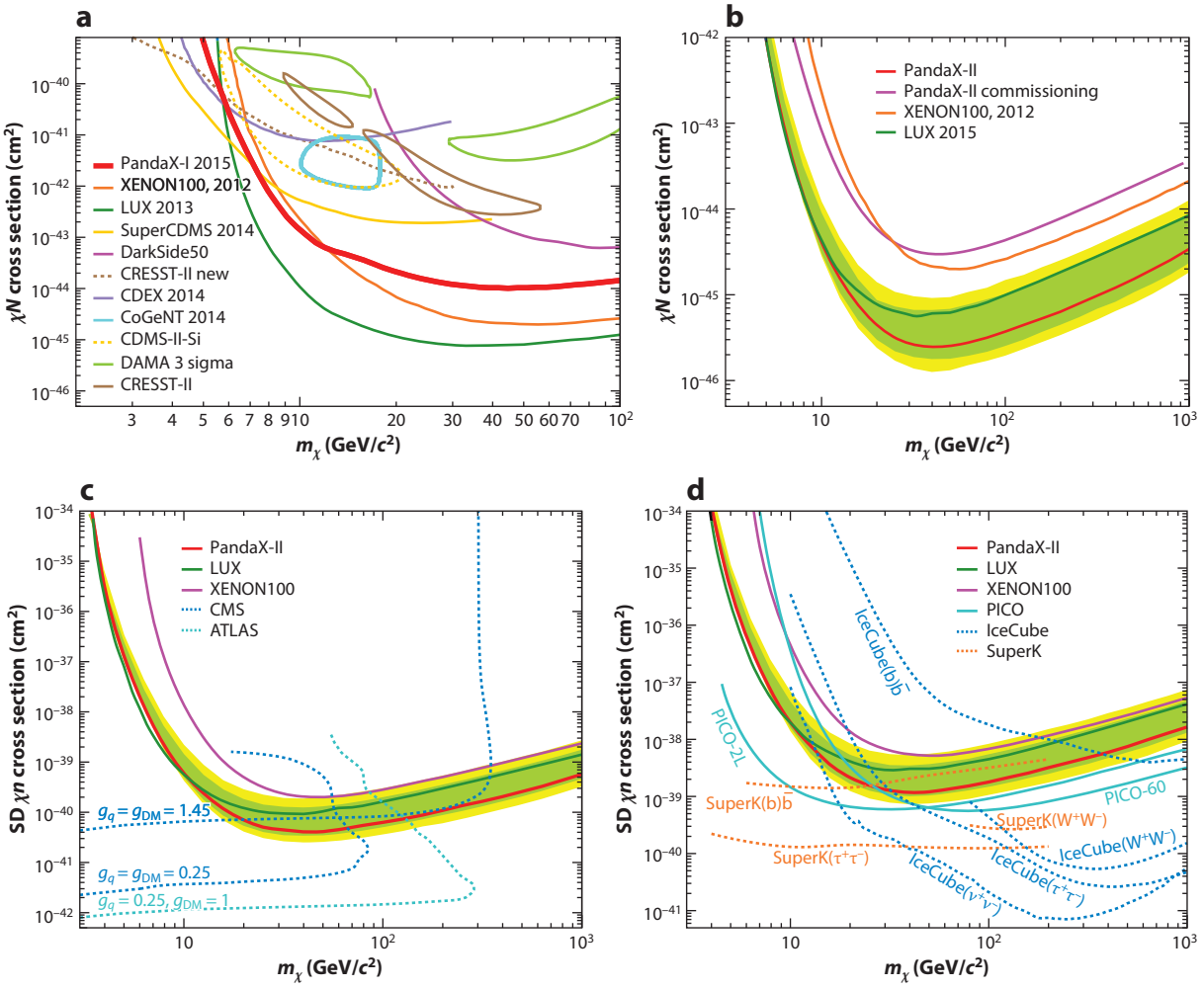

Figure 9

Upper limits at the 90% confidence level (*solid red lines*) set by the PandaX experiments for the weakly interacting massive particle (WIMP)–nucleon (χN) cross sections. (*a*) Limits on the spin-independent χN scattering cross section set by the PandaX-I full exposure data (50), compared with the world data. (*b*) Limits on the spin-independent χN scattering cross section set by the PandaX-II data with 3.3×10^4 kg·day exposure in 98.7 live days (54). (*c*) Limits on the spin-dependent WIMP–neutron (χn) scattering cross section set by the same PandaX-II data set as in panel *b* (55). (*d*) Limits on the spin-dependent WIMP–proton (χp) scattering cross section set by the same PandaX-II data set as in panel *b* (55).

After the data quality cuts, the S1 and S2 signal range cut, and the boosted decision tree cut were applied to the collected data, 389 candidates in the fiducial volume were selected from among 2.45×10^7 events (**Figure 8*a***). No WIMP candidates were observed (**Figure 8*b***).

On the basis of a profile likelihood analysis of all data, an exclusion limit on the spin-independent χN cross section was obtained (**Figure 9*b***). The most stringent limit, 2.5×10^{-46} cm^2 at a WIMP mass of 40 GeV/c^2, represents an improvement of more than a factor of 10 from the limit in Reference 49. In the high-WIMP-mass region, the bounds improve by more than a factor of two over the previous most stringent limit from LUX (56).

By using the same data set, PandaX-II set new constraints on the spin-dependent χn (**Figure 9*c***) and WIMP–proton (χp) (**Figure 9*d***) cross sections. Compared with other direct detection experiments, PandaX-II has derived the most stringent upper limits on the χN cross sections for WIMPs with masses above 10 GeV/c^2.

4.2. Current Efforts and Future Goals

PandaX-II is anticipated to continue physics data taking until 2018, increasing the exposure by a factor of five. In parallel, a future PandaX-xT dark matter experiment and a PandaX-III (57) $0\nu\beta\beta$ experiment are being planned. Both experiments will be located in Hall B of CJPL-II, in which a large, ultrapure water pool will be used as shielding for both experiments. **Figure 6*b*** shows the conceptual layout of the planned experiments.

The PandaX-xT experiment will be a multiton dark matter experiment employing the same dual-phase xenon TPC technology as PandaX-I and -II. Its ultimate goal is to reach the so-called neutrino floor at a sensitivity of $\sim 10^{-49}$ cm^2 for the spin-independent χN cross section at a WIMP mass of $\sim$100 GeV/c^2. The plan of the initial stage of PandaX-xT is to construct a detector with a sensitive target mass of 4 tons of liquid xenon. The TPC will be of a cylindrical shape roughly 1.2 m in diameter and height, almost a factor of two larger in every dimension in comparison to PandaX-II. For the photosensor coverage, it will use in total more than 350 3-inch PMTs at the top and bottom. The powerful self-shielding from liquid xenon will significantly suppress detector material–related background. The level of ^{85}Kr background is also expected to be greatly decreased through online distillation during detector operation. The total background rate is projected to be 0.05×10^{-3} events (kg·day)$^{-1}$, a factor of 40 lower than the best level achieved by PandaX-II. With a 2-year exposure, the sensitivity to the χN cross section is expected to reach 10^{-47} cm^2, more than one order of magnitude lower than the current PandaX-II limit.

Increasing the detector size increases the technological complexity. For example, larger electrodes require new ways to maintain their rigidity and flatness when the electric field is applied, while maintaining the thin wire plane to ensure high photon detection efficiency. As another example, more readout channels and longer readout windows are required, demanding a more sophisticated data acquisition system capable of handling the increased data bandwidth. Therefore, the 4-ton experiment will also serve to demonstrate the critical technology necessary for the future PandaX-xT detector.

The PandaX-III experiment will search for $0\nu\beta\beta$ events using high-pressure gas detectors with enriched ^{136}Xe. In the first phase of PandaX-III, a gaseous TPC with 200 kg of 90%-enriched ^{136}Xe will operate at 10-bar pressure, with a charge readout plane made of microbulk micromesh gaseous structure (micromegas) detectors. It will be the first 100-kg-stage $0\nu\beta\beta$ experiment to be hosted in China. In addition to having good energy and spatial resolution, the TPC will be able to reconstruct tracks from $0\nu\beta\beta$ events, leading to powerful background suppression.

With a single 200-kg module, the half-life sensitivity to ^{136}Xe $0\nu\beta\beta$ decay will reach 10^{26} years after 3 years of operation. With multiple modules with improved background levels and energy resolution, this program could be upgraded to a ton-scale experiment with a half-life sensitivity of 10^{27} years, which would enable the discovery of $0\nu\beta\beta$ if neutrinos are Majorana fermions with the inverted mass ordering.

5. LOW-BACKGROUND FACILITIES

Table 2 summarizes measurements of ambient radiation background by the main experiment hall in CJPL-I. Standard detector techniques (12, 58–60) were adopted to perform these measurements.

Table 2 Summary of the environmental radiation background measurements at the main experiment hall of CJPL-I

Background radioactivity	Detection techniques	Measurement results
Cosmic-muon flux (12)	Plastic scintillator telescope	$(2.0 \pm 0.4) \times 10^{-10}$ cm^{-2} s^{-1}
Radioactivity of bedrock (58)	In situ high-purity germanium detector	
^{238}U series		3.69–4.21 Bq kg^{-1}
^{232}Th series		0.52–0.64 Bq kg^{-1}
^{40}K		4.28 Bq kg^{-1}
Radioactivity of concrete (58)	In situ high-purity germanium detector	
^{238}U series		
^{214}Pb		19.88 Bq kg^{-1}
^{214}Bi		16.03 Bq kg^{-1}
^{232}Th series		
^{228}Ac		7.38 Bq kg^{-1}
^{212}Pb		7.48 Bq kg^{-1}
^{208}Tl		8.15 Bq kg^{-1}
^{40}K		36.67 Bq kg^{-1}
Air absorbed dose rate	Ionization chamber	
Main hall		19.27 nGy h^{-1}
Inside polyethylene room		0.43 nGy h^{-1}
Air radon concentration	Ionization chamber for α counting	
December 2010–September 2011 (59)		
Unventilated		101 ± 14 Bq m^{-3}
Ventilated		86 ± 25 Bq m^{-3}
January 2015–December 2015		
Unventilated (January–March)		108 ± 50 Bq m^{-3}
Ventilated (April–December)		45 ± 28 Bq m^{-3}
Neutron		
Thermal neutron	^{3}He-proportional tube (60)	$(4.00 \pm 0.08) \times 10^{-6}$ cm^{-2} s^{-1}
	Multiple Bonner spheres (61)	$(7.03 \pm 1.81) \times 10^{-6}$ cm^{-2} s^{-1}
Fast neutron	Liquid scintillator	$(1.50 \pm 0.07) \times 10{-}7$ cm^{-2} s^{-1}
	Multiple Bonner spheres (61)	$(3.63 \pm 2.77) \times 10^{-6}$ cm^{-2} s^{-1}
Total neutron flux	Multiple Bonner spheres (61)	$(2.69 \pm 1.02) \times 10^{-5}$ cm^{-2} s^{-1}

The residual cosmic-ray flux at CJPL is $(2.0 \pm 0.4) \times 10^{-10}$ cm^{-2} s^{-2} or, equivalently, ~5 m^{-2} month^{-1}, measured with two groups of triple-layer plastic scintillator telescopes (12). Owing to the large rock overburden, the attenuation factor of 10^{-8} relative to the typical cosmic-ray fluxes on the surface is the largest of all operational underground laboratories (**Figure 2**).

The γ-ray radioactivity from the bedrock, as well as the concrete components of CJPL-I, were measured with an in situ HPGe detector (**Table 2**) (58). The bedrock of Jinping Mountain is mainly marble, providing relatively good radiopurity. The measured radioactivity levels compare favorably with those of other underground laboratories (10, 11).

The materials used to build CJPL-I were adapted from the construction of the nearby hydropower station, and no radioactivity screening procedures were performed. Consequently, the radioactivity levels of the CJPL-I concrete are higher than those of other operational underground laboratories. In the construction of CJPL-II (discussed in Section 6), radioactivity from various concrete samples was measured, and only those with low radiopurity were selected.

The absorbed dose rate in air is 19.27 nGy h^{-1}, as determined with a high-pressure ionization chamber. This dose rate is lower than typical levels at surface locations. Therefore, low-dose-rate calibration for radiation environment dosimetry can be performed at CJPL-I.

The air radon concentration in the main experiment hall at CJPL-I is monitored with commercial ionization detectors. During the early operation of CJPL-I from December 2010 to September 2011, the radon concentration was 101 ± 14 Bq m^{-3} without ventilation, and 86 ± 25 Bq m^{-3} when the ventilation system was fully operational. In 2015, improvements in the ventilation systems resulted in a reduced level of 45 ± 28 Bq m^{-3} or 108 ± 50 Bq m^{-3} when the ventilation was on or off, respectively. Occasionally, there was a sudden surge of radon concentration to several hundred becquerels per cubic meter despite the ventilation system being fully operational. The cause of these surges is unknown and is under investigation.

Neutron backgrounds are measured by multiple detector systems to match their different energy ranges. A gaseous ^{3}He proportional ionization chamber housed in a 100-cm-long tube enables measurements of a thermal neutron flux of $(4.00 \pm 0.08) \times 10^{-6}$ cm^{-2} s^{-1}. A 30-L liquid scintillator loaded with gadolinium tags the fast neutron background via delayed coincidence of proton recoils followed by thermal neutron capture, enabling measurements of $(1.50 \pm 0.07) \times 10^{-7}$ cm^{-2} s^{-1} in the main hall of CJPL-I. A multiple Bonner sphere neutron spectrometer, with ^{3}He ionization chambers enclosed in polyethylene shielding of varying thickness, is used to measure neutron spectra below 20 MeV. The total flux is $(2.69 \pm 1.02) \times 10^{-5}$ cm^{-2} s^{-1}, of which $(7.03 \pm 1.81) \times 10^{-6}$ cm^{-2} s^{-1} consists of thermal (below 0.5 eV) neutrons and $(3.63 \pm 2.77) \times 10^{-6}$ cm^{-2} s^{-1} consists of fast neutrons.

Neutron measurements are also performed inside the polyethylene shielding room in the main CJPL-I hall. The thermal neutron flux is $(1.75 \pm 0.27) \times 10^{-7}$ cm^{-2} s^{-1}, as determined with a ^{3}He proportional ionization chamber, whereas the fast neutron flux is $(4.27 \pm 0.72) \times 10^{-9}$ cm^{-2} s^{-1}, as determined with gadolinium-loaded liquid scintillator. These measurements demonstrate that the 100-cm-thick polyethylene room can efficiently attenuate the neutron flux.

Efficient low-level counting facilities are essential for underground experiments. Currently there are two low-background counting facilities, GeTHU-I and GeTHU-II, which employ HPGe detectors installed within custom-designed shielding structures (8). The best integrated background rate achieved to date is 0.42 counts min^{-1} $(kg \cdot Ge)^{-1}$ between 40 and 2,700 keV. The copper shielding of these germanium detector systems contains residual radioactivity. Future upgrades would reduce the background by use of fine radiopure electroformed copper, instead of commercially produced copper. The GeTHU systems provide support for the various CJPL experiments.

6. CHINA JINPING UNDERGROUND LABORATORY: PHASE II

The commissioning of CJPL-I and the development of its scientific programs attracted great interest both domestically and internationally. Construction on the expansion of the facility began in 2014. **Figure 10** depicts a schematic diagram of the second phase of CJPL (CJPL-II). The key dimension parameters characterizing access to and installation of future experiments are summarized in **Table 3**.

CJPL-II is located 500 m west of CJPL-I, along the same road tunnel. It will have four caverns, each with dimensions of 14 m (width) × 14 m (height) × 130 m (length), that will be interconnected with access and safety tunnels. The laboratory floor area will be approximately 20,000 m^2. Two pits will provide additional headroom for specific applications—one with diameter 18 m and height 18 m and another with length 27 m, width 16 m, and depth 14 m. The total space, including internal traffic tunnels and common facilities, will be approximately 300,000 m^3. It is anticipated

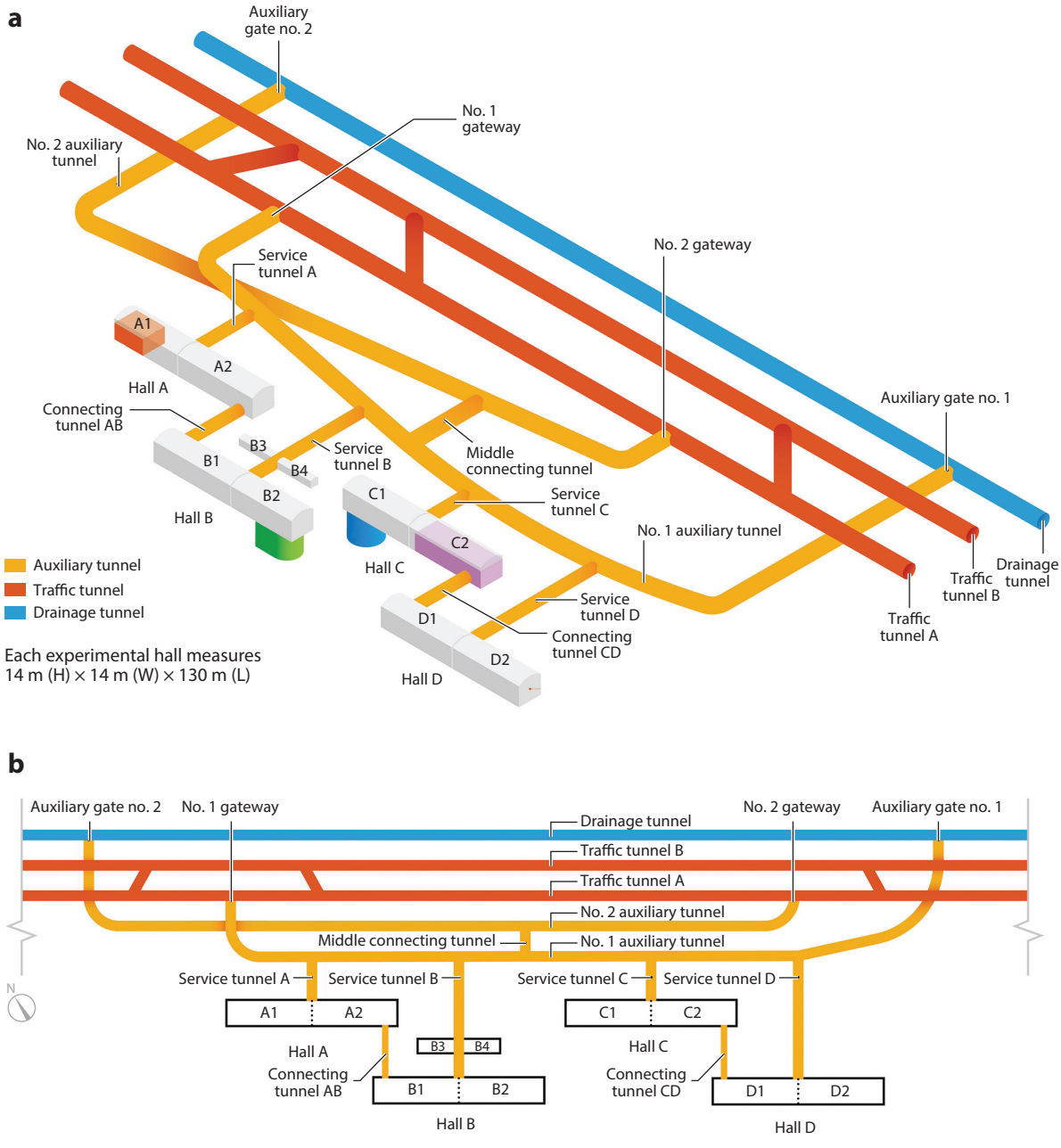

Figure 10

Schematic layout of CJPL-II, showing the four experimental halls as well as the connecting and service tunnels.

Table 3 Summary of the key dimensions of CJPL-II that are relevant to access to and installation of experimental hardware

Items	Dimensions	Description
Main road tunnels	Height, 8 m Width, 8 m	Two parallel tunnels, 9.2 (8.3) km from the east (west) entrance
Internal tunnel	Height, 8 m Width, 8 m Length, 800 m	Connects one of the main tunnels with the experimental halls
Connecting tunnels	Height, 8 m Width, 8 m	One for each hall, 64 m and 134 m from the internal tunnel
Experimental halls	Height, 14 m Width, 14 m Length, 130 m	Four halls in total, entrances at middle sections
Hall B pit	Length, 27 m Width, 16 m Depth, 14 m	
Hall C pit	Diameter, 18 m Depth, 18 m	

that additional ground laboratory, offices, meeting venues, and logistical support will be built before 2020 to allow 150 scientists to live and work on a campus in the neighborhood of another 600 workers from the hydropower company.

Excavation of CJPL-II was performed through drilling and blasting. The walls are supported by numerous steel bolts, and the surfaces are finished with custom-selected low-activity concrete. The potential problems of water underground were alleviated by numerous embedded 5-cm-diameter drain tubes, which guide the water into a drainage system. Representative photographs taken during construction of CJPL-II are displayed in **Figure 11**.

The available electrical power is 10 MW, provided by the Jinping Power Plant. Good ventilation is crucial not only for the workers' health but also for the performance of the equipment and for radon control. Fresh air will be brought in from the western entrance of the Jinping Tunnel by three 800-mm-diameter polyvinyl chloride (PVC) tubes at specified and maximal flow rates of 24,000 $m^3\ h^{-1}$ and 45,000 $m^3\ h^{-1}$, respectively. The peak water supply capacity is 1,006 $m^3\ h^{-1}$.

The potential science programs at CJPL-II are in various stages of development. Both CDEX and PandaX have plans to expand and pursue studies of dark matter and $0\nu\beta\beta$ with detector mass targeted toward the scale of 1 ton of germanium and 10 tons of xenon, respectively. The proposed Jinping Neutrino Experiment (62) will study solar and geoneutrinos (63) with a 4-kiloton liquid scintillator detector. A 1-ton prototype (64) is being constructed.

The approved JUNA (Jinping Underground Laboratory for Nuclear Astrophysics) program (65) will exploit the ultralow-background conditions of CJPL to apply accelerator-based, low-energy nuclear physics techniques to directly study, for the first time, a number of crucial astrophysical nuclear interactions at energies relevant to the evolution of hydrostatic stars. The experimental setup includes a high-current accelerator based on an electron cyclotron resonance (ECR) source (66), advanced detectors, and low-background shielding systems; it will occupy half of Hall A of CJPL-II. The schematic layout is depicted in **Figure 6*c***. The goals of the first phase of JUNA are direct measurements of $^{25}Mg(p,\gamma)^{26}Al$, $^{19}F(p,\alpha)^{16}O$ (67), $^{13}C(\alpha,n)^{16}O$, and

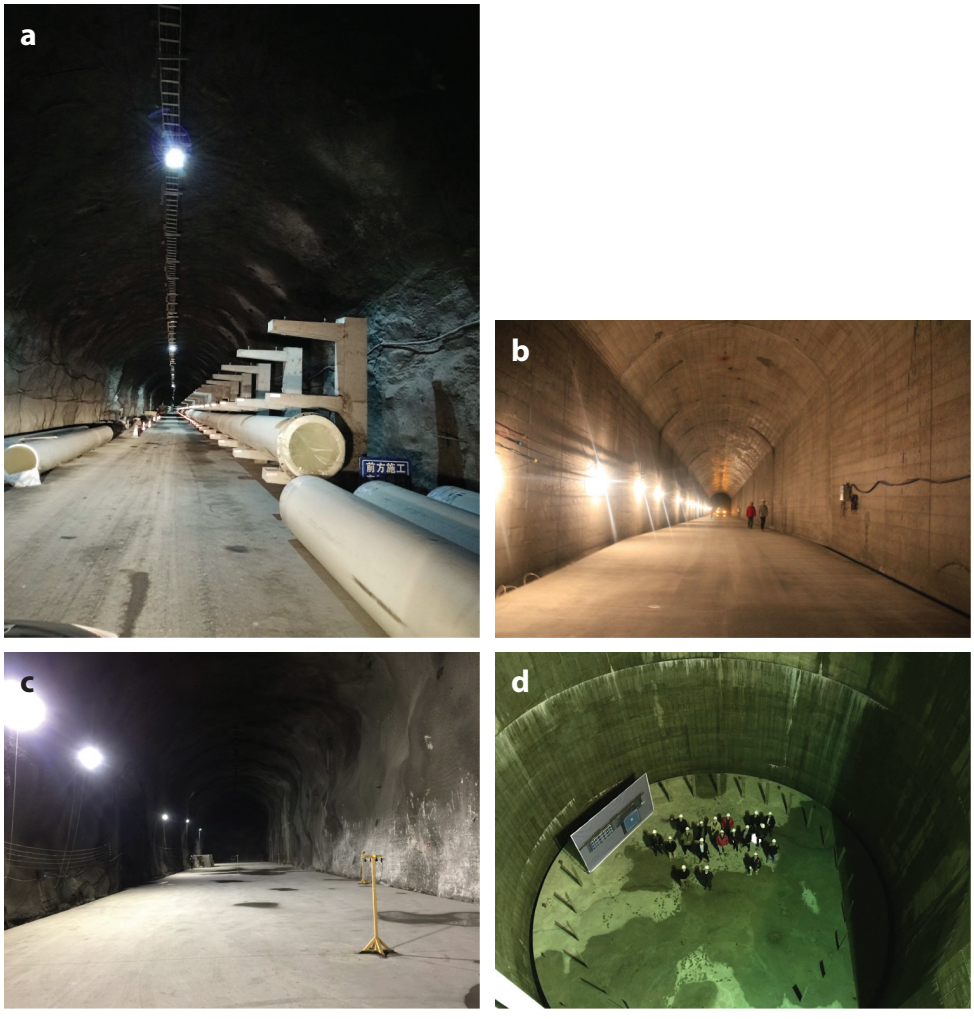

Figure 11

Representative photograph taken during construction of CJPL-II. (*a*) Installation of the ventilation pipes. (*b*) The connecting road tunnel. (*c*) A view of one of the main halls from its middle section toward one end. (*d*) The 18-m-deep pit of Hall C.

$^{12}C(\alpha,\gamma)^{16}O$ cross sections. The experiment will be installed and commissioned on site in 2018, and the initial series of scientific results are expected to become available in 2019.

As the deepest underground laboratory in the world, CJPL also offers an ideal location to study geoscience. Plans have been drawn to build an international open research platform at CJPL-II to explore the interaction of deep-rock mechanics with seismology dynamics, to pursue research on in situ rock-mass testing methods and pressured coring techniques, and to investigate advanced theories of rock mechanics (68). By unveiling the characteristics of the irregular constitutive behaviors of deep rock, such studies would contribute to the safe and efficient excavation of mineral resources as well as to effective disaster prevention.

Rock excavation and civil engineering of CJPL-II finished in May 2016. When construction is completed, the facility will become available to domestic and international researchers. A dedicated

task force will be responsible for the everyday operation and maintenance of the laboratory. An international advisory committee had been in place since 2014 to provide recommendations concerning the management, operation, and potential science programs of CJPL-II.

7. PROSPECTS AND OUTLOOK

CJPL, a new underground facility in Sichuan, China, was constructed within a relatively short period of 8 years. The location has the deepest rock overburden for cosmic-ray suppression in the world. By the time CJPL-II is completed in 2017, it will also have the largest volume of available laboratory space. The facility's horizontal drive-in access enables efficient deployment of large teams and equipment. The existing surface support facilities benefit from the infrastructure created during the earlier construction of hydropower projects in the area. The facility will contribute significantly to the world's capability to conduct low-count-rate experiments.

The two first-generation research programs at CJPL-I, CDEX and PandaX, focus on searches for dark matter. Competitive results on the world stage have been achieved. These projects will continue to evolve in the forthcoming CJPL-II, extending and expanding the scope of their physics programs to include other areas of study, such as $0\nu\beta\beta$. A new program on low-count-rate nuclear astrophysics measurements, JUNA, is in preparation.

There remains plenty of space for prospective future users at CJPL-II. The science programs are still in the formative stage. The facility has attracted a great deal of user interest, both nationally and internationally. The research community looks forward to the evolution of the ideas and projects under way at CJPL.

DISCLOSURE STATEMENT

The authors are not aware of any affiliations, memberships, funding, or financial holdings that might be perceived as affecting the objectivity of this review.

ACKNOWLEDGMENTS

The authors thank all of their scientific colleagues and technical staff who contributed to the realization of the facility and science programs reported in this review. Construction and operation of CJPL are financed by the National Natural Science Foundation of China (11355001), and basic facility funding is provided by the Ministry of Education of China. Funding support for the CDEX program is provided by the National Natural Science Foundation of China (11275107, 11355001, 11475117, and 11475099) and the National Basic Research Program of China (973 Program) (2010CB833006). The PandaX program is supported by grants from the National Science Foundation of China (11435008, 11455001, 11505112, and 11525522). We greatly appreciate the contributions of Xun Chen, Xia Li, Shin-Ted Lin, Shu-Kui Liu, and Li-Tao Yang to the preparation of this review.

LITERATURE CITED

1. Lesko KT. *AIP Conf. Proc.* 1672:020002 (2015)
2. Olive K, et al. *Chin. Phys. C* 38:090001 (2014)
3. Kang KJ, et al. *J. Phys. Conf. Ser.* 203:012028 (2010)
4. Li J, Ji X, Haxton W, Wang JS. *Phys. Proc.* 61:576 (2015)
5. Kang KJ, et al. *Front. Phys.* 8:412 (2013)

6. Yue Q, Kang K, Li J, Wong HT. *J. Phys. Conf. Ser.* 718:042066 (2016)
7. Cao X, et al. *Sci. China Phys. Mech. Astron.* 57:1476 (2014)
8. Zeng Z, et al. *Appl. Radiat. Isot.* 91:165 (2014)
9. Shiyong W, Manbin S, Jian W. *Bull. Eng. Geol. Environ.* 69:325 (2010)
10. Votano L. *Eur. Phys. J. Plus* 127:109 (2012)
11. Smith NJT. *Eur. Phys. J. Plus* 127:108 (2012)
12. Wu YC, et al. *Chin. Phys. C* 37:086001 (2013)
13. Narasimhan VS. *Proc. Indian Natl. Sci. Acad.* 70:11 (2004)
14. Qian Y, et al. *High Energy Phys. Nucl. Phys.* 28:877 (2004)
15. Wong HT, et al. *J. Phys. Conf. Ser.* 39:266 (2006)
16. Luke P, Goulding F, Madden N, Pehl R. *IEEE Trans. Nucl. Sci.* 36:926 (1989)
17. Barbeau PS, Collar JI, Tench O. *J. Cosmol. Astropart. Phys.* 2007:009 (2007)
18. Soma A, et al. *Nucl. Instrum. Methods A* 836:67 (2016)
19. Aalseth CE, et al. *Phys. Rev. Lett.* 106:131301 (2011)
20. Aalseth CE, et al. *Phys. Rev. D* 88:012002 (2013)
21. Lin ST, et al. *Phys. Rev. D* 79:061101(R) (2009)
22. Li HB, et al. *Phys. Rev. Lett.* 110:261301 (2013)
23. Giovanetti G, et al. *Phys. Proc.* 61:77 (2015)
24. Zhao W, et al. *Phys. Rev. D* 93:092003 (2016)
25. Liu SK, et al. *Phys. Rev. D* 90:032003 (2014)
26. Kang KJ, et al. *Chin. Phys. C* 37:126002 (2013)
27. Zhao W, et al. *Phys. Rev. D* 88:052004 (2013)
28. Li HB, et al. *Astropart. Phys.* 56:1 (2014)
29. Yue Q, et al. *Phys. Rev. D* 90:091701(R) (2014)
30. Bernabei R, et al. *Eur. Phys. J. C* 73:2648 (2013)
31. Savage C, Gelmini G, Gondolo P, Freese K. *J. Cosmol. Astropart. Phys.* 2009:010 (2009)
32. Agnese R, et al. *Phys. Rev. Lett.* 111:251301 (2013)
33. Agnese R, et al. *Phys. Rev. Lett.* 112:041302 (2014)
34. Agnese R, et al. *Phys. Rev. Lett.* 116:071301 (2016)
35. Angloher G, et al. *Eur. Phys. J. C* 76:25 (2016)
36. Akerib DS, et al. *Phys. Rev. Lett.* 112:091303 (2014)
37. Akerib DS, et al. *Phys. Rev. Lett.* 116:161302 (2016)
38. Ahmed Z, et al. *Phys. Rev. Lett.* 106:131302 (2011)
39. Kim JE, Carosi G. *Rev. Mod. Phys.* 82:557 (2010)
40. Liu SK, et al. *Phys. Rev. D* 95:052006 (2017)
41. Armengaud E, et al. *J. Cosmol. Astropart. Phys.* 11:067 (2013)
42. Aprile E, et al. *Phys. Rev. D* 90:062009 (2014)
43. Wang L et al. arXiv:1703.01877 [hep-ex] (2017)
44. Angle J, et al. *Phys. Rev. Lett.* 107:051301 (2011)
45. Aprile E, et al. *Phys. Rev. Lett.* 109:181301 (2012)
46. Akimov DY, et al. *Phys. Lett. B* 709:14 (2012)
47. Gong H, et al. *J. Instrum.* 8:P01002 (2013)
48. Xiao M, et al. *Sci. China Phys. Mech. Astron.* 57:2024 (2014)
49. Tan A, et al. *Phys. Rev. D* 93:122009 (2016)
50. Xiao X, et al. *Phys. Rev. D* 92:052004 (2015)
51. Bernabei R, et al. *Eur. Phys. J. C* 56:333 (2008)
52. Bernabei R, et al. *Eur. Phys. J. C* 67:39 (2010)
53. Angloher G, et al. *Eur. Phys. J. C* 72:1971 (2012)
54. Tan A, et al. *Phys. Rev. Lett.* 117:121303 (2016)
55. Fu C, et al. *Phys. Rev. Lett.* 118:071301 (2017)
56. Akerib DS, et al. *Phys. Rev. Lett.* 116:161301 (2016)
57. Chen X, et al. arXiv:1610.08883 [physics] (2016)
58. Zeng Z, et al. *J. Radioanal. Nucl. Chem.* 301:443 (2014)

59. Mi YH, et al. *China Sci. Pap.* 10:2783 (2015)
60. Zeng Z, Gong H, Yue Q, Li J. *Nucl. Instrum. Methods A* 804:108 (2015)
61. Hu Q, et al. arXiv:1612.04054 [physics] (2016)
62. Beacom JF, et al. *Chin. Phys. C* 41:023002 (2017)
63. Wan LY, Hussain G, Wang Z, Chen SM. *Phys. Rev. D* 95:053001 (2017)
64. Wang ZY, et al. *Nucl. Instrum. Methods A* 855:81 (2017)
65. Liu W, et al. *Sci. China Phys. Mech. Astron.* 59:642001 (2016)
66. Wu Q, et al. *Nucl. Instrum. Methods A* 830:214 (2016)
67. He JJ, et al. *Sci. China Phys. Mech. Astron.* 59:652001 (2016)
68. Xie HP. *Adv. Eng. Sci.* 49:2 (in Chinese) (2017)